INTERNATIONAL JOURNAL FOR NUMERICAL METHODS IN FLUIDS
Int. J. Numer. Meth. Fluids 2010; **62**:1107–1133
Published online 22 April 2009 in Wiley InterScience (www.interscience.wiley.com). DOI: 10.1002/fld.2057

Realization of contact resolving approximate Riemann solvers for strong shock and expansion flows

Sung Don Kim[1], Bok Jik Lee[1], Hyoung Jin Lee[1], In-Seuck Jeung[1,2,*,†] and Jeong-Yeol Choi[3]

[1]*School of Mechanical and Aerospace Engineering, Seoul National University, Seoul 151-744, Korea*
[2]*Institute of Advanced Aerospace Technology, Seoul National University, Seoul 151-744, Korea*
[3]*Department of Aerospace Engineering, Pusan National University, Busan 609-735, Korea*

SUMMARY

The Harten–Lax–van Leer contact (HLLC) and Roe schemes are good approximate Riemann solvers that have the ability to resolve shock, contact, and rarefaction waves. However, they can produce spurious solutions, called shock instabilities, in the vicinity of strong shock. In strong expansion flows, the Roe scheme can admit nonphysical solutions such as expansion shock, and it sometimes fails. We carefully examined both schemes and propose simple methods to prevent such problems. High-order accuracy is achieved using the weighted average flux (WAF) and MUSCL-Hancock schemes. Using the WAF scheme, the HLLC and Roe schemes can be expressed in similar form. The HLLC and Roe schemes are tested against Quirk's test problems, and shock instability appears in both schemes. To remedy shock instability, we propose a control method of flux difference across the contact and shear waves. To catch shock waves, an appropriate pressure sensing function is defined. Using the proposed method, shock instabilities are successfully controlled. For the Roe scheme, a modified Harten–Hyman entropy fix method using Harten–Lax–van Leer-type switching is suggested. A suitable criterion for switching is established, and the modified Roe scheme works successfully with the suggested method. Copyright © 2009 John Wiley & Sons, Ltd.

Received 25 July 2008; Revised 4 November 2008; Accepted 27 February 2009

KEY WORDS: HLLC scheme; Roe scheme; shock instability; modified Harten Hyman entropy fix; HLLC–HLL; Roe–HLLE

1. INTRODUCTION

High-resolution shock-capturing schemes require stable and sharp resolution of discontinuities with high accuracy. Shock-capturing schemes are generally upwind-based schemes and are usually based

*Correspondence to: In-Seuck Jeung, School of Mechanical and Aerospace Engineering, Seoul National University, Seoul 151-744, Korea.
†E-mail: enjis@snu.ac.kr

Contract/grant sponsor: SNU
Contract/grant sponsor: Korea government (MEST); contract/grant number: R01-2008-000-12362-0

on the local Riemann problem. One of the popular shock-capturing methods is the Godunov-type scheme. Godunov assumed that conservative variables are piecewise constant over the mesh cells at each time step, and the time-averaged flux function is determined by the exact solution of the local Riemann problem at the cell interface [1]. The original Godunov scheme is first-order accurate and hence highly dissipative. In addition, an iterative method is required because the Riemann problem has no closed form solution [1]. Approximate state Riemann solvers do not need iterative processes and hence are more useful. Extensive studies have been conducted to develop Godunov-type schemes. We examined two approximate Riemann solvers with second-order extension of the weighted average flux (WAF) and MUSCL-Hancock schemes. The Harten–Lax–van Leer contact (HLLC) and Roe schemes have good shock-capturing ability, and they also have good contact and shear wave resolving properties.

For the Roe scheme, a number of problems have been reported [2, 3] and special modification studies have been conducted [3–5]. Quirk catalogued a number of situations in which the Roe scheme can give unreliable results in multi-dimensional flows [3]; these include expansion shock, negative internal energy, slowly moving shock, the carbuncle phenomenon, kinked Mach stem, and odd–even decoupling. The so-called shock instability and nonexistence of a solution for strong expansion flows are major problems in such failings. Entropy violating conditions are also a well-known problem in the Roe scheme. Many researchers try to overcome these entropy violating solutions using entropy correction [2, 6, 7].

For shock instability problems, previous researchers have shown that Riemann solvers that resolve the contact and shear waves exactly have problems in the vicinity of strong shock waves. Quirk suggested a strategy to use combined fluxes so that a dissipative scheme, such as the Harten–Lax–van Leer–Einfeldt (HLLE) scheme, is used in the shock region [3]. Liou analyzed several Riemann solvers by expressing numerical fluxes in terms of mass flux. He defined the dissipative terms in the mass flux of each scheme, and identified the dissipative terms that are responsible for shock instability [8]. Liou controlled the magnitude of $|\lambda_2|$ in the Roe scheme to make the pressure difference term have a value of zero in the dissipative terms of the mass flux; thus, the instability was eliminated.

Quirk also described the problems in the strong expansion condition. He used the HLLE scheme to eliminate the expansion shock appearance in the test problem of supersonic corner flows.

This paper is focused on shock instability and strong expansion problems. Our main interest is the modification of the HLLC and Roe schemes to remedy the previously described problems. The main concept of this paper is to control the resolution of the contact and shear waves in the vicinity of strong shock waves using an appropriate pressure sensing function. In addition, to avoid the problems of the Roe scheme in strong expansion flows, we use the Harten–Hyman entropy fix method with Harten–Lax–van Leer (HLL)-type scheme switching. HLL-type schemes have no problem in strong expansion flow, and they can be used as an alternative method. A suitable criterion to estimate the survival of the Roe scheme is presented. Beyond the limits of such estimation, the HLL-type scheme is used and it shows good results.

2. APPROXIMATE RIEMANN SOLVERS

The Godunov method is to find solution of the Riemann problem, which may be the exact solution or an approximate solution. Approximate solutions considered in this paper are the HLL, HLLE, HLLC, and Roe schemes, which are explicit approximate solutions. Figure 1 shows the structure of

DOI: 10.1002/fld

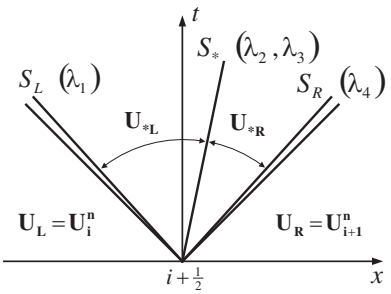

Figure 1. Structure of the solution of the Riemann problem with data $\mathbf{U}_\mathbf{i}^\mathbf{n}$ and $\mathbf{U}_\mathbf{i+1}^\mathbf{n}$.

the Riemann problem for the x-split two-dimensional Euler equations [1]. There are three waves and four separate constant states. Pressure and normal velocity are constant in the star region across the middle wave. Middle wave S_* has the multiplicity 2 of the eigenvalue u. The λ_2 field is associated with contact discontinuity and density jumps discontinuously. There is a new characteristic field associated with λ_3. This corresponds to a shear wave in which the tangential velocity component v changes. The λ_2 and λ_3 fields are linearly degenerate, and the λ_1 and λ_4 characteristic fields are genuinely nonlinear and are associated with rarefaction and shock waves [1].

To solve the multi-dimensional nonlinear systems of hyperbolic conservation laws, we employed a finite volume approach. For nonCartesian grids, a rotating and rotate-back method is used.

2.1. HLL and HLLC schemes

Harten, Lax, van Leer presented a direct approximation of the numerical flux to compute Godunov flux [9]. The resulting HLL Riemann solver consists of two waves with three constant states. The HLL Riemann solver is very efficient and robust, and gives a physical, entropy-satisfying solution. The HLL scheme can be applied directly to Euler equations without any modifications. However, the two-wave assumption is incorrect in Euler equations. The resolution of contact and shear waves can be very inaccurate. Toro *et al.* HLLC scheme is a modification of the HLL scheme whereby the missing contacts and shear waves are restored [10]. The HLLC scheme is the simplest solver to preserve shock, contact, and shear waves exactly. Batten *et al.* have shown that the HLLC scheme is positively conservative [11].

HLL intercell flux is written as [1, 9]

$$\mathbf{F}_{\mathbf{i+1/2}}^{\mathrm{HLL}} = \begin{cases} \mathbf{F_L}, & 0 \leqslant S_L \\ \mathbf{F}_{*\mathbf{L}} = \mathbf{F_L} + S_L(\mathbf{U}^{\mathrm{HLL}} - \mathbf{U_L}), & S_L \leqslant 0 \leqslant S_* \\ \mathbf{F}_{*\mathbf{R}} = \mathbf{F_R} - S_R(\mathbf{U_R} - \mathbf{U}^{\mathrm{HLL}}), & S_* \leqslant 0 \leqslant S_R \\ \mathbf{F_R}, & 0 \geqslant S_R \end{cases} \tag{1}$$

where S_L is the smallest wave speed and S_R is the largest wave speed.

The constant state (star region) vector $\mathbf{U}^{\mathrm{HLL}}$ is the average of the exact Riemann problem between the slowest and fastest waves [1, 9]:

$$\mathbf{U}^{\mathrm{HLL}} = \frac{S_R\mathbf{U_R} - S_L\mathbf{U_L} + \mathbf{F_L} - \mathbf{F_R}}{S_R - S_L} \tag{2}$$

DOI: 10.1002/fld

Because the HLL scheme assumes a two-wave system, $\mathbf{F}_{*\mathbf{L}}$ and $\mathbf{F}_{*\mathbf{R}}$ are the same as HLL flux $\mathbf{F}^{\mathrm{HLL}}$:

$$\mathbf{F}^{\mathrm{HLL}} = \frac{S_R\mathbf{F_L} - S_L\mathbf{F_R} + S_R S_L(\mathbf{U_R} - \mathbf{U_L})}{S_R - S_L} \tag{3}$$

The HLLC intercell flux is written as [1, 10]

$$\mathbf{F}^{\mathrm{HLLC}}_{\mathbf{i+1/2}} = \begin{cases} \mathbf{F_L}, & 0 \leqslant S_L \\ \mathbf{F}_{*\mathbf{L}} = \mathbf{F_L} + S_L(\mathbf{U}_{*\mathbf{L}} - \mathbf{U_L}), & S_L \leqslant 0 \leqslant S_* \\ \mathbf{F}_{*\mathbf{R}} = \mathbf{F_R} - S_R(\mathbf{U_R} - \mathbf{U}_{*\mathbf{R}}), & S_* \leqslant 0 \leqslant S_R \\ \mathbf{F_R}, & 0 \geqslant S_R \end{cases} \tag{4}$$

$\mathbf{U}_{*\mathbf{L}}$ and $\mathbf{U}_{*\mathbf{R}}$ are the conserved variable vectors in the star region between the smallest and largest wave speeds. $\mathbf{F}_{*\mathbf{L}}$ and $\mathbf{F}_{*\mathbf{R}}$ are obtained by applying Rankine–Hugoniot conditions across the each of the waves [1].

The HLL and HLLC schemes require the estimation of the smallest, largest, and middle wave speeds in the Riemann problem. To obtain wave speeds for the HLLC scheme, we use the pressure–velocity-based wave speed estimation of Toro [1].

The HLL scheme is usually used in a combined form. The HLL scheme in a single formula is expressed as [12]

$$\mathbf{F}^{\mathrm{HLL}}_{\mathbf{i+1/2}} = \frac{b^+}{b^+ - b^-}\mathbf{F_L} - \frac{b^-}{b^+ - b^-}\mathbf{F_R} + \frac{b^+ b^-}{b^+ - b^-}(\mathbf{U_R} - \mathbf{U_L}) \tag{5}$$

where

$$b^+ = \max(0, b^R), \quad b^- = \min(0, b^L) \tag{6}$$

Numerical wave speeds b^R and b^L of the HLL scheme are written as [1, 12]

$$b^L = S_L, \quad b^R = S_R \tag{7a}$$

Einfeldt *et al.* proposed the wave speed motivated by the Roe-averaged values $\tilde{u}_n$ and $\tilde{a}$ [4]. Using the following wave speed, the HLL scheme is often called the HLLE scheme [1, 4, 12]:

$$b^L = \min(S_L, \tilde{u}_n - \tilde{a}), \quad b^R = \max(S_R, \tilde{u}_n + \tilde{a}) \tag{7b}$$

The subscript n implies the normal component at the cell interface.

The HLLC scheme can also be expressed in a single formula:

$$\mathbf{F}^{\mathrm{HLLC}}_{\mathbf{i+1/2}} = C_1\mathbf{F_L} + C_2\mathbf{F_R} + A(\mathbf{U}_{*\mathbf{L}} - \mathbf{U_L}) + B(\mathbf{U}_{*\mathbf{R}} - \mathbf{U_R}) \tag{8}$$

Coefficients C_1, C_2, A, and B are defined as follows:

$$C_1 = \frac{\max(0, S_*)}{S_*}, \quad C_2 = \frac{\min(0, S_*)}{S_*} \tag{9a}$$

$$A = S_L\left(C_1 - \frac{\max(0, S_L)}{S_L}\right), \quad B = S_R\left(C_2 - \frac{\min(0, S_R)}{S_R}\right) \tag{9b}$$

DOI: 10.1002/fld

When S_* approaches zero, C_1 and C_2 are determined as follows:

$$|S_*|<\varepsilon, \quad \begin{cases} S_*>0, & C_1=1.0, \quad C_2=0.0 \\ S_*<0, & C_1=0.0, \quad C_2=1.0 \end{cases} \tag{10}$$

ε is chosen to be 10^{-16}.

2.2. Roe scheme

In the original Roe scheme, the average Jacobian matrix $\tilde{\mathbf{A}}$ is first sought to find averaged eigenvalues, right eigenvectors, and wave strengths [13]. In the Roe–Pike method, the construction of $\tilde{\mathbf{A}}$ is avoided and scalar quantities are obtained by direct averages [1]. In this paper, The Roe–Pike method is used instead of the original Roe method.

According to the sign of the waves, the numerical flux of the Roe scheme is expressed as the one-sided formula [14]:

$$\mathbf{F_{i+1/2}}=\mathbf{F_L}+\sum_{\tilde{\lambda}_k\leqslant 0}\tilde{\alpha}_k\tilde{\lambda}_k\tilde{\mathbf{K}}^{(k)} \quad \text{or} \quad \mathbf{F_{i+1/2}}=\mathbf{F_R}-\sum_{\tilde{\lambda}_k\geqslant 0}\tilde{\alpha}_k\tilde{\lambda}_k\tilde{\mathbf{K}}^{(k)} \tag{11}$$

Alternatively, they can be written by the averaged formula [14]

$$\mathbf{F_{i+1/2}}=\frac{1}{2}(\mathbf{F_L}+\mathbf{F_R})-\frac{1}{2}\sum_{k=1}^{m}\tilde{\alpha}_k|\tilde{\lambda}_k|\tilde{\mathbf{K}}^{(k)} \tag{12}$$

Data and flux differences are expressed with the wave strengths $\tilde{\alpha}_k$, eigenvalues $\tilde{\lambda}_k$, and the right eigenvectors $\tilde{\mathbf{K}}^{(k)}$ [14]:

$$\mathbf{\Delta U}^{(k)}=\tilde{\alpha}_k\tilde{\mathbf{K}}^{(k)}, \quad \mathbf{\Delta F}^{(k)}=\tilde{\alpha}_k\tilde{\lambda}_k\tilde{\mathbf{K}}^{(k)}=\tilde{\lambda}_k\mathbf{\Delta U}^{(k)} \tag{13}$$

Each flux difference is expressed as

$$\mathbf{\Delta F}^{(1)}=\tilde{\alpha}_1\tilde{\lambda}_1\tilde{\mathbf{K}}^{(1)}=\tilde{\lambda}_1\mathbf{\Delta U}^{(1)}=\mathbf{F_{*L}}-\mathbf{F_L} \tag{14a}$$

$$\mathbf{\Delta F}^{(2)}=\tilde{\alpha}_2\tilde{\lambda}_2\tilde{\mathbf{K}}^{(2)}+\tilde{\alpha}_3\tilde{\lambda}_3\tilde{\mathbf{K}}^{(3)}=\mathbf{F_{*R}}-\mathbf{F_{*L}} \tag{14b}$$

$$\mathbf{\Delta F}^{(3)}=\tilde{\alpha}_4\tilde{\lambda}_4\tilde{\mathbf{K}}^{(4)}=\tilde{\lambda}_4\mathbf{\Delta U}^{(4)}=\mathbf{F_R}-\mathbf{F_{*R}} \tag{14c}$$

The second flux difference is related to the wave jumps $\tilde{\alpha}_2\tilde{\lambda}_2\tilde{\mathbf{K}}^{(2)}$ and $\tilde{\alpha}_3\tilde{\lambda}_3\tilde{\mathbf{K}}^{(3)}$. From the first and the third flux differences, $\mathbf{F_{*L}}$ and $\mathbf{F_{*R}}$ can be expressed by the first and last wave strengths, eigenvalues, and right eigenvectors. This expression gives a simple way of extending the procedure to three-dimensional flows [15]:

$$\mathbf{F_{*L}}=\mathbf{F_L}+\tilde{\alpha}_1\tilde{\lambda}_1\tilde{\mathbf{K}}^{(1)}=\mathbf{F_L}+\tilde{\lambda}_1\mathbf{\Delta U}^{(1)}=\mathbf{F_L}+\tilde{\lambda}_1(\mathbf{U_{*L}}-\mathbf{U_L}) \tag{15a}$$

$$\mathbf{F_{*R}}=\mathbf{F_R}-\tilde{\alpha}_4\tilde{\lambda}_4\tilde{\mathbf{K}}^{(4)}=\mathbf{F_R}-\tilde{\lambda}_4\mathbf{\Delta U}^{(4)}=\mathbf{F_R}-\tilde{\lambda}_4(\mathbf{U_R}-\mathbf{U_{*R}}) \tag{15b}$$

DOI: 10.1002/fld

The first and last wave strengths and right eigenvectors are [1]

$$\tilde{\alpha}_1 = \frac{1}{2\tilde{a}^2}[\Delta p - \tilde{\rho}\tilde{a}\Delta u_n], \quad \tilde{\alpha}_4 = \frac{1}{2\tilde{a}^2}[\Delta p + \tilde{\rho}\tilde{a}\Delta u_n] \tag{16}$$

$$\tilde{\mathbf{K}}^{(1)} = [1,\ \tilde{u}_n - \tilde{a},\ \tilde{u}_t,\ \tilde{H} - \tilde{u}_n\tilde{a}]^{\mathrm{T}} \tag{17a}$$

$$\tilde{\mathbf{K}}^{(4)} = [1,\ \tilde{u}_n + \tilde{a},\ \tilde{u}_t,\ \tilde{H} + \tilde{u}_n\tilde{a}]^{\mathrm{T}} \tag{17b}$$

All fluxes across the waves in the Riemann fan (Figure 1) are expressed with the first and last wave strengths, eigenvalues, right eigenvectors, and the left and right fluxes.

2.3. Entropy fix of the Roe scheme

The linearized Riemann problem solution consists only of discontinuous jumps, and they are good approximations for the shocks and contacts. However, the rarefaction waves have continuous changes. Therefore, the linearized Riemann problem solution has difficulties when the rarefaction wave is transonic or sonic. In that situation, nonphysical, entropy violating discontinuous waves can appear. Harten and Hyman presented a modification to eliminate such entropy violating discontinuities [16]. It is a well-known entropy fix method, and the Roe scheme satisfies the entropy condition with it. Einfeldt *et al.* analyzed the characteristics of low internal energy flows [4]. He showed that the reason for the failure of the Roe scheme is the underestimated numerical wave speeds. In linearized solvers, all wave speeds are obtained from a single-averaged state. Wave speeds obtained in such a manner will, in general, underestimate the true expansion wave velocity [17]. Negative internal energies and expansion shocks appear under such conditions. In expansion flows, a physically admissible discontinuity of speed S requires $S_{\mathrm{T}} \geqslant S \geqslant S_{\mathrm{H}}$, where S_{H} and S_{T} are head and tail wave speeds, respectively.

In this paper, we used the Harten–Hyman entropy fix modified by Toro [1]. Figure 2 shows the left transonic rarefaction case [1]. A new state $\mathbf{U_{SL}}$ is introduced, and a single jump $(\mathbf{U_{*L}} - \mathbf{U_L})$ with speed $\tilde{\lambda}_1$ is split into two jumps, $(\mathbf{U_{SL}} - \mathbf{U_L})$ and $(\mathbf{U_{*L}} - \mathbf{U_{SL}})$, with speeds λ_1^L and λ_1^R. The

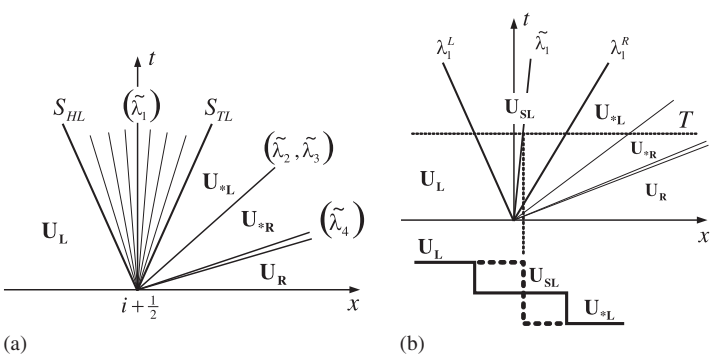

Figure 2. Harten–Hyman Entropy fix: (a) left transonic rarefaction waves and (b) entropy fix for left transonic rarefaction wave.

DOI: 10.1002/fld

resulting new eigenvalue is expressed as [1]

$$\bar{\lambda}_1 = \lambda_1^L \left(\frac{\lambda_1^R - \tilde{\lambda}_1}{\lambda_1^R - \lambda_1^L} \right) \tag{18a}$$

In the right transonic rarefaction case, the new eigenvalue is [1]

$$\bar{\lambda}_4 = \lambda_4^R \left(\frac{\tilde{\lambda}_4 - \lambda_4^L}{\lambda_4^R - \lambda_4^L} \right) \tag{18b}$$

Toro's version of the Harten–Hyman entropy fix relies on the estimation for particle velocity u_*, sound speeds a_{*L} and a_{*R}, and the head and tail wave speeds of the rarefaction.

In the left transonic case, wave speeds λ_1^L and λ_1^R are expressed as [1]

$$\lambda_1^L = u_L - a_L, \quad \lambda_1^R = u_* - a_{*L} \tag{19a}$$

In the right transonic case, wave speeds λ_4^L and λ_4^R are expressed as [1]

$$\lambda_4^L = u_* + a_{*R}, \quad \lambda_4^R = u_R + a_R \tag{19b}$$

The star values are obtained by the relations $\mathbf{U_{*L}} - \mathbf{U_L} = \tilde{\alpha}_1 \tilde{\mathbf{K}}^{(1)}$ and $\mathbf{U_R} - \mathbf{U_{*R}} = \tilde{\alpha}_4 \tilde{\mathbf{K}}^{(4)}$.

3. HIGH ORDER AND TVD METHOD

3.1. WAF approach

The WAF scheme is the second-order extension of the Godunov first-order upwind method. This is second-order accurate in space and time [1, 18–21]. The WAF scheme appears to give better results than the MUSCL-Hancock scheme, and needs only a very small number of cells to resolve shock and contact [1]. In addition, it has very low numerical diffusion.

In the WAF scheme, the intercell flux is represented by an integral average of the physical flux across the full structure of the solution of a local Riemann problem. The structure of the solution of the Riemann problem with data $\mathbf{U_i^n}$ and $\mathbf{U_i^{n+1}}$ consists of three waves and four constant states. As shown in Figure 3, the integral average of the WAF intercell flux has a summation involving flux terms in regions 1–4 with weights obtained by normalizing lengths A_0A_1 through A_3A_4. Each constant state and the waves are written as [1]

$$S_1 = S_L, \quad S_2 = S_*, \quad S_3 = S_R \tag{20}$$

$$\mathbf{U}^{(1)} = \mathbf{U_i^n}, \quad \mathbf{U}^{(2)} = \mathbf{U_{*L}}, \quad \mathbf{U}^{(3)} = \mathbf{U_{*R}}, \quad \mathbf{U}^{(4)} = \mathbf{U_{i+1}^n} \tag{21}$$

The WAFs are [1]

$$\mathbf{F_{i+1/2}} = \sum_{k=1}^{N+1} \beta_k \mathbf{F_{i+1/2}^{(k)}}, \quad \beta_k = \frac{|A_{k-1}A_k|}{\Delta x}, \quad k = 1, \ldots, 4 \tag{22}$$

DOI: 10.1002/fld

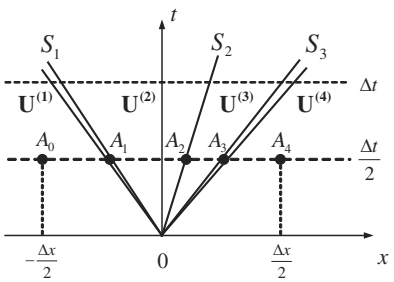

Figure 3. Evaluation of the WAF intercell flux.

Weights β_k are expressed in terms of the wave speed S_k as [1]

$$\begin{aligned} \beta_k &= \tfrac{1}{2}(c_k - c_{k-1}) \\ c_k &= \frac{\Delta t S_k}{\Delta x}, \quad c_k = \text{Courant number for wave } k \text{ of speed } S_k \end{aligned} \tag{23}$$

An alternative form of the flux is written as [1]

$$\mathbf{F_{i+1/2}} = \frac{1}{2}(\mathbf{F_i} + \mathbf{F_{i+1}}) - \frac{1}{2}\sum_{k=1}^{N} c_k \Delta \mathbf{F^{(k)}_{i+1/2}} \tag{24}$$

3.2. TVD version of WAF

Because the WAF scheme is a second-order accurate scheme, spurious oscillations appeared in the vicinity of high gradient.

The TVD modification of the WAF flux with limiter function $\phi^{(k)}_{i+1/2}$ is written as [1]

$$\mathbf{F_{i+1/2}} = \frac{1}{2}(\mathbf{F_i} + \mathbf{F_{i+1}}) - \frac{1}{2}\sum_{k=1}^{N} \text{sign}(c_k)\phi^{(k)}_{i+1/2} \Delta \mathbf{F^{(k)}_{i+1/2}} \tag{25}$$

where

$$\phi^{(k)}_{i+1/2} = \phi_{i+1/2}(r^{(k)}) \tag{26}$$

The flow parameter $r^{(k)}$ is defined by [1]

$$r^{(k)} = \begin{cases} \Delta q^{(k)}_{i-1/2} / \Delta q^{(k)}_{i+1/2}, & c_k > 0 \\ \Delta q^{(k)}_{i+3/2} / \Delta q^{(k)}_{i+1/2}, & c_k < 0 \end{cases} \tag{27}$$

where ρ is selected for a single quantity q [1]. For the limiter function $\phi^{(k)}_{i+1/2}$, the MINBEE limiter is used.

DOI: 10.1002/fld

3.3. Application of WAF to the HLL and HLLC schemes

WAF schemes can be applied directly to the HLL and HLLC approximate Riemann solvers. When we use the HLL or HLLE scheme, the second wave jumps are neglected; hence, there is no difference across the contact and shear waves.

The numerical flux of the HLLC scheme at the intercell boundary is given as [1]

$$\mathbf{F}_{\mathbf{i+1/2}}^{\mathrm{HLLC,WAF}} = \frac{1}{2}(\mathbf{F_L}+\mathbf{F_R}) - \frac{1}{2}\begin{bmatrix} \mathrm{sign}(c_1)\phi^{(1)}(\mathbf{F}_{*\mathbf{L}}-\mathbf{F_L}) \\ +\mathrm{sign}(c_2)\phi^{(2)}(\mathbf{F}_{*\mathbf{R}}-\mathbf{F}_{*\mathbf{L}}) \\ +\mathrm{sign}(c_3)\phi^{(3)}(\mathbf{F_R}-\mathbf{F}_{*\mathbf{R}}) \end{bmatrix} \tag{28}$$

The left and right fluxes in star region are expressed as [1]

$$\mathbf{F}_{*\mathbf{L}} = \mathbf{F_L} + S_L(\mathbf{U}_{*\mathbf{L}} - \mathbf{U_L}) \tag{29a}$$

$$\mathbf{F}_{*\mathbf{R}} = \mathbf{F_R} - S_R(\mathbf{U_R} - \mathbf{U}_{*\mathbf{R}}) \tag{29b}$$

In the HLLC scheme, star region values are obtained with jump conditions across each wave as described by [1]

$$\mathbf{U}_{*\mathbf{K}} = \rho_K\left(\frac{S_K-u_{nK}}{S_K-S_*}\right)\begin{bmatrix} 1 \\ S_* \\ u_{tK} \\ \dfrac{E_K}{\rho_K}+(S_*-u_{nK})\left[S_*+\dfrac{p_K}{\rho_K(S_K-u_{nK})}\right] \end{bmatrix}, \quad K=L \text{ or } R \tag{30}$$

The Courant numbers for wave k are [1]

$$c_1 = S_L\frac{\Delta t}{\Delta x}, \quad c_2 = S_*\frac{\Delta t}{\Delta x}, \quad c_3 = S_R\frac{\Delta t}{\Delta x} \tag{31}$$

The HLL and HLLE schemes can be expressed in a similar manner:

$$\mathbf{F}_{\mathbf{i+1/2}}^{\mathrm{HLL/HLLE,WAF}} = \frac{1}{2}(\mathbf{F_L}+\mathbf{F_R}) - \frac{1}{2}\begin{bmatrix} \mathrm{sign}(c_1)\phi^{(1)}(\mathbf{F}_{*\mathbf{L}}-\mathbf{F_L}) \\ +0 \\ +\mathrm{sign}(c_3)\phi^{(3)}(\mathbf{F_R}-\mathbf{F}_{*\mathbf{R}}) \end{bmatrix} \tag{32}$$

The expressions for $\mathbf{F}_{*\mathbf{L}}$ and $\mathbf{F}_{*\mathbf{R}}$ are same as in the HLLC scheme. Data $\mathbf{U}_{*\mathbf{L}}$ and $\mathbf{U}_{*\mathbf{R}}$ have same value, $\mathbf{U}^{\mathrm{HLL}}$.

3.4. Reinterpretation of the Roe scheme and application of the WAF scheme

Quirk presented second-order extension of the Roe scheme using WAF scheme [15]

$$\mathbf{F}_{\mathbf{i+1/2}}^{\mathrm{RoeWAF,Quirk}} = \frac{1}{2}(\mathbf{F_L}+\mathbf{F_R}) - \frac{1}{2}\sum_{k=1}^{N}\frac{[1-\psi^{(k)}(1-|c_k|)]}{|c_k|}c_k\tilde{\alpha}_k\tilde{\lambda}_k\tilde{\mathbf{K}}^{(k)} \tag{33}$$

DOI: 10.1002/fld

where $\psi^{(k)}$ is the conventional flux limiter. Equation (33) also gives the relation between the WAF limiter function and the conventional limiters.

This relation is also presented by Toro [1]:

$$\phi^{(k)} = 1 - \psi^{(k)}(1 - |c_k|) \tag{34}$$

Equation (33) can be obtained in different point of view. The numerical flux of the Roe scheme in the averaged formula can be expanded as follows:

$$\begin{aligned}\mathbf{F}_{\mathbf{i+1/2}}^{\mathrm{Roe}} &= \frac{1}{2}(\mathbf{F_L}+\mathbf{F_R}) - \frac{1}{2}\sum_{k=1}^{m}\tilde{\alpha}_k|\tilde{\lambda}_k|\tilde{\mathbf{K}}^{(k)} = \frac{1}{2}(\mathbf{F_L}+\mathbf{F_R}) - \frac{1}{2}\sum_{k=1}^{m}\mathrm{sign}(\tilde{\lambda}_k)\tilde{\alpha}_k\tilde{\lambda}_k\tilde{\mathbf{K}}^{(k)} \\ &= \frac{1}{2}(\mathbf{F_L}+\mathbf{F_R}) - \frac{1}{2}\begin{bmatrix}\mathrm{sign}(\tilde{\lambda}_1)(\mathbf{F}_{*\mathbf{L}}-\mathbf{F_L}) \\ \quad +\mathrm{sign}(\tilde{\lambda}_2)(\mathbf{F}_{*\mathbf{R}}-\mathbf{F}_{*\mathbf{L}}) \\ \quad +\mathrm{sign}(\tilde{\lambda}_4)(\mathbf{F_R}-\mathbf{F}_{*\mathbf{R}})\end{bmatrix}\end{aligned} \tag{35}$$

This alternative formula for the Roe scheme can be interpreted as an evenly weighted WAF formulation. Using Equations (34) and (35), no special treatment is needed for the Roe scheme to apply the WAF scheme. Therefore, the resulting Roe scheme in the WAF form can be written as

$$\mathbf{F}_{\mathbf{i+1/2}}^{\mathrm{RoeWAF}} = \frac{1}{2}(\mathbf{F_L}+\mathbf{F_R}) - \frac{1}{2}\begin{bmatrix}\mathrm{sign}(c_1)\phi^{(1)}(\mathbf{F}_{*\mathbf{L}}-\mathbf{F_L}) \\ \quad +\mathrm{sign}(c_2)\phi^{(2)}(\mathbf{F}_{*\mathbf{R}}-\mathbf{F}_{*\mathbf{L}}) \\ \quad +\mathrm{sign}(c_3)\phi^{(3)}(\mathbf{F_R}-\mathbf{F}_{*\mathbf{R}})\end{bmatrix} \tag{36}$$

where

$$\mathbf{F}_{*\mathbf{L}} = \mathbf{F_L} + \tilde{\alpha}_1\tilde{\lambda}_1\tilde{\mathbf{K}}^{(1)}, \quad \mathbf{F}_{*\mathbf{R}} = \mathbf{F_R} - \tilde{\alpha}_4\tilde{\lambda}_4\tilde{\mathbf{K}}^{(4)} \tag{37}$$

$$c_1 = \tilde{\lambda}_1\frac{\Delta t}{\Delta x}, \quad c_2 = \tilde{\lambda}_2\frac{\Delta t}{\Delta x}, \quad c_3 = \tilde{\lambda}_4\frac{\Delta t}{\Delta x} \tag{38}$$

Here, we see that the HLLC and Roe schemes can be written in the same framework using the WAF scheme.

3.5. MUSCL-Hancock method

The MUSCL-Hancock scheme in two-dimensional flow has the following three steps [1]. The first step is to obtain reconstructed data and boundary-extrapolated values. The cell averages $\mathbf{U}_{\mathbf{i,j}}^{\mathbf{n}}$ are reconstructed using slope vectors Δ_i and Δ_j. Then, the boundary-extrapolated values are [1]

$$\mathbf{U}_{\mathbf{i,j}}^{-\mathbf{x}} = \mathbf{U}_{\mathbf{i,j}}^{\mathbf{n}} - \tfrac{1}{2}\Delta_i, \quad \mathbf{U}_{\mathbf{i,j}}^{+\mathbf{x}} = \mathbf{U}_{\mathbf{i,j}}^{\mathbf{n}} + \tfrac{1}{2}\Delta_i \tag{39a}$$

$$\mathbf{U}_{\mathbf{i,j}}^{-\mathbf{y}} = \mathbf{U}_{\mathbf{i,j}}^{\mathbf{n}} - \tfrac{1}{2}\Delta_j, \quad \mathbf{U}_{\mathbf{i,j}}^{+\mathbf{y}} = \mathbf{U}_{\mathbf{i,j}}^{\mathbf{n}} + \tfrac{1}{2}\Delta_j \tag{39b}$$

DOI: 10.1002/fld

The second step is to obtain the evolution of boundary extrapolated values [1]:

$$\hat{\mathbf{U}}^{-\mathbf{x}}_{\mathbf{i,j}} = \mathbf{U}^{-\mathbf{x}}_{\mathbf{i,j}} + \frac{\Delta t}{2\Delta x}[\mathbf{F}(\mathbf{U}^{-\mathbf{x}}_{\mathbf{i,j}}) - \mathbf{F}(\mathbf{U}^{+\mathbf{x}}_{\mathbf{i,j}})] - \frac{\Delta t}{2\Delta y}[\mathbf{G}(\mathbf{U}^{-\mathbf{y}}_{\mathbf{i,j}}) - \mathbf{G}(\mathbf{U}^{+\mathbf{y}}_{\mathbf{i,j}})] \tag{40a}$$

$$\hat{\mathbf{U}}^{+\mathbf{x}}_{\mathbf{i,j}} = \mathbf{U}^{+\mathbf{x}}_{\mathbf{i,j}} + \frac{\Delta t}{2\Delta x}[\mathbf{F}(\mathbf{U}^{-\mathbf{x}}_{\mathbf{i,j}}) - \mathbf{F}(\mathbf{U}^{+\mathbf{x}}_{\mathbf{i,j}})] - \frac{\Delta t}{2\Delta y}[\mathbf{G}(\mathbf{U}^{-\mathbf{y}}_{\mathbf{i,j}}) - \mathbf{G}(\mathbf{U}^{+\mathbf{y}}_{\mathbf{i,j}})] \tag{40b}$$

$$\hat{\mathbf{U}}^{-\mathbf{y}}_{\mathbf{i,j}} = \mathbf{U}^{-\mathbf{y}}_{\mathbf{i,j}} + \frac{\Delta t}{2\Delta x}[\mathbf{F}(\mathbf{U}^{-\mathbf{x}}_{\mathbf{i,j}}) - \mathbf{F}(\mathbf{U}^{+\mathbf{x}}_{\mathbf{i,j}})] - \frac{\Delta t}{2\Delta y}[\mathbf{G}(\mathbf{U}^{-\mathbf{y}}_{\mathbf{i,j}}) - \mathbf{G}(\mathbf{U}^{+\mathbf{y}}_{\mathbf{i,j}})] \tag{40c}$$

$$\hat{\mathbf{U}}^{+\mathbf{y}}_{\mathbf{i,j}} = \mathbf{U}^{+\mathbf{y}}_{\mathbf{i,j}} + \frac{\Delta t}{2\Delta x}[\mathbf{F}(\mathbf{U}^{-\mathbf{x}}_{\mathbf{i,j}}) - \mathbf{F}(\mathbf{U}^{+\mathbf{x}}_{\mathbf{i,j}})] - \frac{\Delta t}{2\Delta y}[\mathbf{G}(\mathbf{U}^{-\mathbf{y}}_{\mathbf{i,j}}) - \mathbf{G}(\mathbf{U}^{+\mathbf{y}}_{\mathbf{i,j}})] \tag{40d}$$

The last step is to obtain the solution of the Riemann problem. At intercell position $(i+\frac{1}{2}, j)$, $\hat{\mathbf{U}}^{+\mathbf{x}}_{\mathbf{i,j}}$ and $\hat{\mathbf{U}}^{-\mathbf{x}}_{\mathbf{i+1,j}}$ are used as left and right values to obtain the solution $\mathbf{U}_{\mathbf{i+1/2,j}}$ [1].

4. SHOCK INSTABILITY AND ITS CURE

Quirk concluded that any Godunov scheme built on a single Riemann solver has shortcomings and sometimes fails [3]. Therefore, he suggested the combination method with the dissipative scheme. Liou suggested that the cause of such failings can be described as a transverse numerical instability associated with the shock wave, and called it 'shock instability' [8]. A simple test can be carried out to validate Liou's suggestion for Quirk's odd–even grid perturbation problem. The centerline of the grid is perturbed from a perfectly uniform grid by $\pm 10^{-6}$, and the grid size is 801×21. A moving shock of $M_s = 6$ propagates down a duct. Previous researchers have shown that the HLLE scheme is free from shock instability. Therefore, the HLLE scheme is applied only to one direction to see the directional effect. Figure 4 shows the density contour at $X_s \sim 300$. In the left column of Figure 4, the HLLE scheme is applied to the numerical flux in the x-direction. The decoupling becomes progressively worse as the shock propagates down the duct. In the right column of Figure 4, the numerical flux in the y-direction is determined by the HLLE scheme.

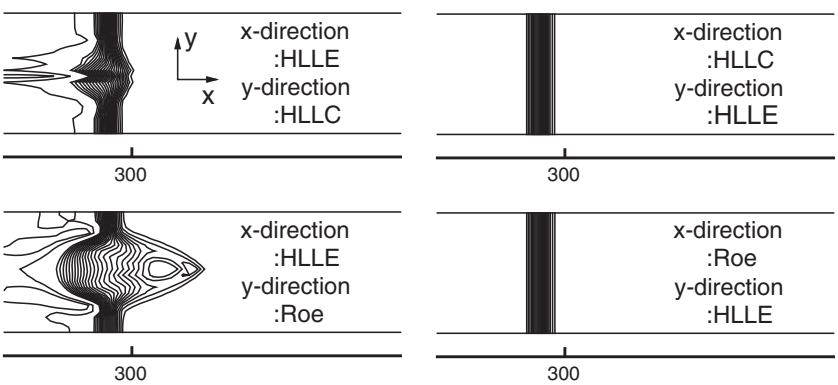

Figure 4. Odd–even decoupling occurrence according to the direction of HLLE application.

DOI: 10.1002/fld

In this case, the dissipative scheme is applied in the transverse direction of the shock wave, and odd–even decoupling is completely eliminated. It shows that shock instability can be removed when the dissipative scheme is applied in the transverse direction of the shock wave.

Liou analyzed the structure of the numerical diffusivity of several numerical flux schemes [8]. In his analysis, the dissipation term is further expanded in terms of differences of primitive variables ρ, $\mathbf{u}$, and p. He then defined the dissipation coefficients of density difference $D^{(\rho)}$ and pressure difference $D^{(p)}$ and showed the roles of the dissipation coefficients of the AUSM+, AUSMDV, HLLE, and Roe scheme. Different schemes have different representations for $D^{(\rho)}$ and $D^{(p)}$. He confirmed that the root of the shock instability is the dissipative pressure term in the mass flux. Liou presented the following lemma: 'A scheme having the property $D^{(p)}=0$ in the mass flux is a shock-stable scheme.' Quirk employed the HLLE scheme in the vicinity of a strong shock using a localized switching function. Although the HLLE scheme is a low-resolution scheme, it resolves isolated shocks as well as an exact Riemann solver [3]. By Liou's analysis, the HLLE scheme has the property of $D^{(p)}=0$. Pandolfi and D'Ambrosio reported that 'methods that explicitly deal with the contact surface display a clear evidence of carbuncle phenomenon; if the interaction is very weak, or totally ignored, no carbuncle instability occurs' [22]. From the previous studies and the results of Figure 4, we can see that shock instability is related to the resolution of the contact and shear waves. Therefore, we propose a new approach to control shock instability with a simple adjustment of the flux differences across the middle wave of the Riemann problem. Our suggested method is applied to the HLLC and Roe schemes.

4.1. Numerical mass fluxes in the Roe and HLLC schemes

Liou expressed numerical fluxes in terms of the mass flux and defined dissipation terms in the mass flux to analyze the root of shock instability in each scheme [8]. For the Roe scheme, centrally weighted average $\langle \dot{m} \rangle$ and dissipation coefficients in mass flux are expressed as follows [8]:

$$\langle \dot{m} \rangle = \tfrac{1}{2}(\rho_L u_{nL} + \rho_R u_{nR}) \tag{41a}$$

$$D^{(\rho)} = |\tilde{\lambda}_2| \tag{41b}$$

$$D^{(p)} = \frac{1}{2\tilde{a}^2}(|\tilde{\lambda}_1| + |\tilde{\lambda}_5| - 2|\tilde{\lambda}_2|) \tag{41c}$$

Liou showed that a scheme which has the property of $D^{(p)}=0$ is the shock stable scheme. The Roe scheme has $D^{(p)} \neq 0$ and thus cannot avoid shock instability. In Liou's analysis, mass flux is only used in the continuity equation because the Roe scheme does not fit in the general mass flux form. For the HLLC scheme, the same process is applied. Mass flux is only applied in the continuity equation of the HLLC flux. Using the single formula of the HLLC scheme presented in Section 2.1 (see Equation (8)), the flux of the continuity equation is expressed as follows:

$$f^{\text{HLLC}}_{(\text{continuity})} = C_1 \rho_L u_{nL} + C_2 \rho_R u_{nR} + A\left(\rho_L \frac{S_L - u_{nL}}{S_L - S_*} - \rho_L\right) + B\left(\rho_R \frac{S_R - u_{nR}}{S_R - S_*} - \rho_R\right) \tag{42}$$

The dissipation term of the continuity equation is given by

$$D^{\text{HLLC}}_{(\text{continuity})} = A\rho_L \frac{S_* - u_{nL}}{S_L - S_*} + B\rho_R \frac{S_* - u_{nR}}{S_R - S_*} \tag{43}$$

DOI: 10.1002/fld

The preceding expression does not contain any pressure difference terms. However, the estimated wave speed of the middle wave S_* contains a pressure difference term as follows:

$$S_* = \frac{p_R - p_L + \rho_L u_{nL}(S_L - u_{nL}) - \rho_R u_{nR}(S_R - u_{nR})}{\rho_L(S_L - u_{nL}) - \rho_R(S_R - u_{nR})} \tag{44}$$

The pressure difference term in S_* is written as

$$\frac{1}{\rho_L(S_L - u_{nL}) - \rho_R(S_R - u_{nR})}\Delta p \tag{45}$$

The HLLC scheme also has a nonzero pressure difference term and it cannot avoid shock instability.

4.2. New approach to remedy shock instability

We propose a new approach to remedy shock instability in the framework of the HLLC approximate Riemann solver by defining an appropriate blending function. By reducing the data jump across the middle wave, the three-wave system approaches a two-wave system, and hence approaches the property of the HLL scheme. Figure 5 shows the proposed method of controlling the second data jump, $\mathbf{U}_{*\mathbf{R}} - \mathbf{U}_{*\mathbf{L}}$, across the middle wave to remedy shock instability.

A reference data state is selected as an integral average of the exact solution of the Riemann problem $\mathbf{U}^{\mathrm{HLL}}$ between the smallest and the largest waves at time T.

Introducing the function f and reference data state $\mathbf{U}^{\mathrm{HLL}}$, the second data jump $\mathbf{U}_{*\mathbf{R}} - \mathbf{U}_{*\mathbf{L}}$ is split into two parts: $f \cdot (\mathbf{U}^{\mathrm{HLL}} - \mathbf{U}_{*\mathbf{L}})$ and $f \cdot (\mathbf{U}_{*\mathbf{R}} - \mathbf{U}^{\mathrm{HLL}})$. Whenever the function f has a value below unity, the HLL scheme blends automatically with the original contact resolving scheme.

Left and right fluxes in the star region are now defined by newly obtained data of states $\mathbf{U}_{*\mathbf{L}}^{\mathrm{new}}$ and $\mathbf{U}_{*\mathbf{R}}^{\mathrm{new}}$:

$$\mathbf{F}_{*\mathbf{L}}^{\mathrm{new}} = \mathbf{F}_{\mathbf{L}} + S_L(\mathbf{U}_{*\mathbf{L}}^{\mathrm{new}} - \mathbf{U}_{\mathbf{L}}) \tag{46a}$$

$$\mathbf{F}_{*\mathbf{R}}^{\mathrm{new}} = \mathbf{F}_{\mathbf{R}} - S_R(\mathbf{U}_{\mathbf{R}} - \mathbf{U}_{*\mathbf{R}}^{\mathrm{new}}) \tag{46b}$$

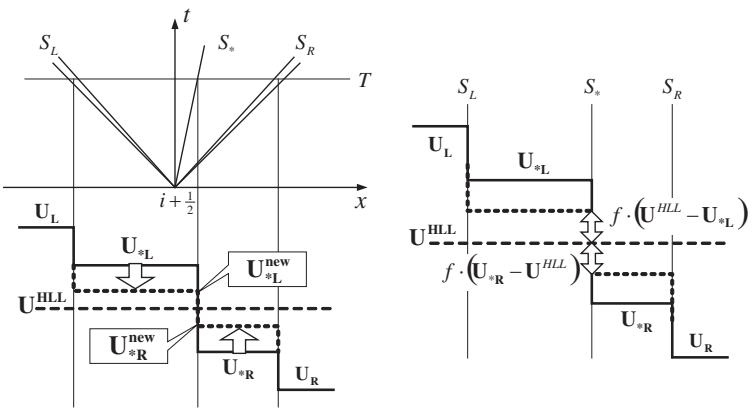

Figure 5. Controlled data jump quantities across the middle wave to remedy shock instability.

DOI: 10.1002/fld

The new data states $\mathbf{U}_{*\mathbf{L}}^{\text{new}}$ and $\mathbf{U}_{*\mathbf{R}}^{\text{new}}$ are obtained as follows:

$$\mathbf{U}_{*\mathbf{L}}^{\text{new}} = f \cdot \mathbf{U}_{*\mathbf{L}} + (1-f) \cdot \mathbf{U}^{\text{HLL}} \tag{47a}$$

$$\mathbf{U}_{*\mathbf{R}}^{\text{new}} = f \cdot \mathbf{U}_{*\mathbf{R}} + (1-f) \cdot \mathbf{U}^{\text{HLL}} \tag{47b}$$

The resulting data of states $\mathbf{U}_{*\mathbf{L}}^{\text{new}}$ and $\mathbf{U}_{*\mathbf{R}}^{\text{new}}$ can be applied directly in the HLLC method. For the Roe scheme, the new data states can also be applied to the reinterpreted formulation in Section 3.4 (see Equations (35) and (36)).

4.3. Blending function f

The previously proposed procedure must be applied in the vicinity of shock. Therefore, a blending function is needed which catches only shock waves. Quirk used the following function in the guise of a mesh refinement monitor function to identify the required cell interfaces [3]:

$$\frac{|p_R - p_L|}{\min(p_R, p_L)} > \alpha, \quad \alpha\text{: user-defined value} \tag{48}$$

The user-defined value α must be supplied to use Quirk's function. We define the blending function in the form of the inverse of Quirk's function, and it is limited to unity.

A new function f is expressed as follows:

$$f = \frac{\min(p_R, p_L)}{|p_R - p_L| + \varepsilon} \quad \text{limitation } f \leqslant 1.0 \tag{49}$$

ε is chosen to be 10^{-16}.

p_R and p_L are the pressures that act on the cell interface. From the definition of the new data states $\mathbf{U}_{*\mathbf{L}}^{\text{new}}$ and $\mathbf{U}_{*\mathbf{R}}^{\text{new}}$ (Equations (47a) and (47b)), the function f should be lower than unity. Except shock waves, the pressure changes continuously and the pressure difference $p_R - p_L$ across the cell interface is not large. Therefore, the blending function has a value of 1.0 in most computational domain. In the vicinity of the shock waves, the pressure difference is increased and the blending function has a meaningful value.

Figure 6 shows the normal shock relations and corresponding blending function profile. From a pressure ratio of 2, the blending function is activated and shows a sharp decrease as the pressure ratio is increased and approaches zero.

As shown in Figure 4, shock instability occurred by the transferred perturbation in the transverse direction of the shock. Therefore, all the neighboring intercells must be examined [5]. Figure 7 shows the required surfaces to identify cell surfaces for the blending function in the x- and y-direction numerical flux calculations.

$$f_x = \min(f_{i+1/2,j}, f_{i,j+1/2}, f_{i,j-1/2}, f_{i+1,j+1/2}, f_{i+1,j-1/2}) \tag{50a}$$

$$f_y = \min(f_{i,j+1/2}, f_{i-1/2,j}, f_{i+1/2,j}, f_{i-1/2,j+1}, f_{i+1/2,j+1}) \tag{50b}$$

4.4. HLLC scheme with HLL blending in WAF formulation

For the HLLC scheme, the proposed method is applied directly without any modification. Our method only controls the data at the star region, and wave speeds are not changed. Wave speeds are

DOI: 10.1002/fld

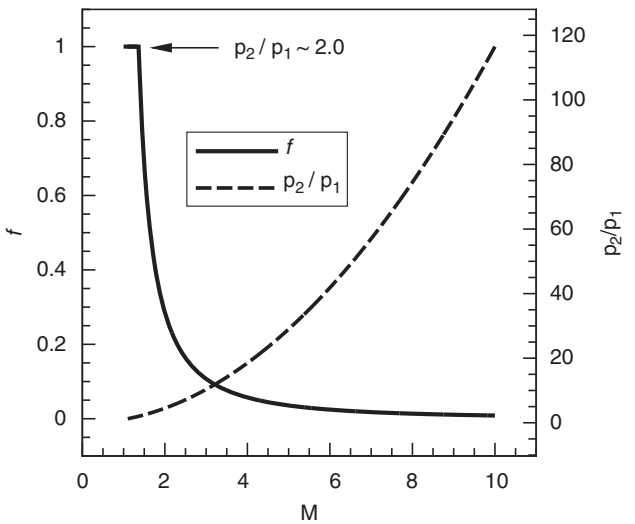

Figure 6. Normal shock relation and blending function.

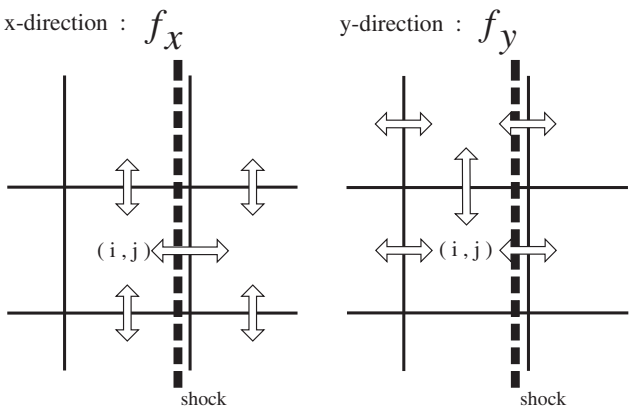

Figure 7. Required surfaces to identify cell surfaces for blending function.

physical wave speeds obtained using the pressure–velocity-based wave speed estimation method of Toro. This method is named HLLC–HLL for convenience. The resulting HLLC–HLL scheme in the WAF form can be written as

$$\mathbf{F}_{\mathbf{i+1/2}}^{\mathrm{HLLC-HLL,WAF}} = \frac{1}{2}(\mathbf{F_L}+\mathbf{F_R}) - \frac{1}{2}\begin{bmatrix} \mathrm{sign}(c_1)\phi^{(1)}(\mathbf{F}_{*\mathbf{L}}^{\mathrm{HLLC-HLL}} - \mathbf{F_L}) \\ +\mathrm{sign}(c_2)\phi^{(2)}(\mathbf{F}_{*\mathbf{R}}^{\mathrm{HLLC-HLL}} - \mathbf{F}_{*\mathbf{L}}^{\mathrm{HLLC-HLL}}) \\ +\mathrm{sign}(c_3)\phi^{(3)}(\mathbf{F_R} - \mathbf{F}_{*\mathbf{R}}^{\mathrm{HLLC-HLL}}) \end{bmatrix} \tag{51}$$

DOI: 10.1002/fld

Newly defined fluxes $\mathbf{F}_{*\mathbf{L}}^{\mathrm{HLLC-HLL}}$ and $\mathbf{F}_{*\mathbf{R}}^{\mathrm{HLLC-HLL}}$ are expressed as follows:

$$\mathbf{F}_{*\mathbf{L}}^{\mathrm{HLLC-HLL}} = \mathbf{F}_{\mathbf{L}} + S_L(\mathbf{U}_{*\mathbf{L}}^{\mathrm{HLLC-HLL}} - \mathbf{U}_{\mathbf{L}}) \tag{52a}$$

$$\mathbf{F}_{*\mathbf{R}}^{\mathrm{HLLC-HLL}} = \mathbf{F}_{\mathbf{R}} - S_R(\mathbf{U}_{\mathbf{R}} - \mathbf{U}_{*\mathbf{R}}^{\mathrm{HLLC-HLL}}) \tag{52b}$$

where

$$\mathbf{U}_{*\mathbf{L}}^{\mathrm{HLLC-HLL}} = \mathbf{U}_{*\mathbf{L}}^{\mathrm{new}} \tag{53a}$$

$$\mathbf{U}_{*\mathbf{R}}^{\mathrm{HLLC-HLL}} = \mathbf{U}_{*\mathbf{R}}^{\mathrm{new}} \tag{53b}$$

4.5. Roe scheme with HLLE blending in WAF formulation

In the Roe scheme, wave speeds are expressed in terms of Roe-averaged values. The HLLE scheme also uses Roe-averaged values to estimate wave speeds. As the function f has a value below the unity, the HLLE scheme blends with the Roe scheme. The Roe scheme with HLLE blending is named Roe–HLLE:

$$\mathbf{F}_{\mathbf{i+1/2}}^{\mathrm{Roe-HLLE,WAF}} = \frac{1}{2}(\mathbf{F}_{\mathbf{L}} + \mathbf{F}_{\mathbf{R}}) - \frac{1}{2}\begin{bmatrix} \mathrm{sign}(c_1)\phi^{(1)}(\mathbf{F}_{*\mathbf{L}}^{\mathrm{Roe-HLLE}} - \mathbf{F}_{\mathbf{L}}) \\ \quad +\mathrm{sign}(c_2)\phi^{(2)}(\mathbf{F}_{*\mathbf{R}}^{\mathrm{Roe-HLLE}} - \mathbf{F}_{*\mathbf{L}}^{\mathrm{Roe-HLLE}}) \\ \quad +\mathrm{sign}(c_3)\phi^{(3)}(\mathbf{F}_{\mathbf{R}} - \mathbf{F}_{*\mathbf{R}}^{\mathrm{Roe-HLLE}}) \end{bmatrix} \tag{54}$$

Newly defined fluxes $\mathbf{F}_{*\mathbf{L}}^{\mathrm{Roe-HLLE}}$ and $\mathbf{F}_{*\mathbf{R}}^{\mathrm{Roe-HLLE}}$ are expressed as follows:

$$\mathbf{F}_{*\mathbf{L}}^{\mathrm{Roe-HLLE}} = \mathbf{F}_{\mathbf{L}} + \tilde{\lambda}_1(\mathbf{U}_{*\mathbf{L}}^{\mathrm{Roe-HLLE}} - \mathbf{U}_{\mathbf{L}}) \tag{55a}$$

$$\mathbf{F}_{*\mathbf{R}}^{\mathrm{Roe-HLLE}} = \mathbf{F}_{\mathbf{R}} - \tilde{\lambda}_4(\mathbf{U}_{\mathbf{R}} - \mathbf{U}_{*\mathbf{R}}^{\mathrm{Roe-HLLE}}) \tag{55b}$$

The newly defined data states $\mathbf{U}_{*\mathbf{L}}^{\mathrm{Roe-HLLE}}$ and $\mathbf{U}_{*\mathbf{R}}^{\mathrm{Roe-HLLE}}$ are expressed with eigensystem values:

$$\mathbf{U}_{*\mathbf{L}}^{\mathrm{Roe-HLLE}} = f \cdot \mathbf{U}_{*\mathbf{L}}^{\mathrm{Roe}} + (1-f) \cdot \mathbf{U}^{\mathrm{HLL}} \tag{56a}$$

$$\mathbf{U}_{*\mathbf{R}}^{\mathrm{Roe-HLLE}} = f \cdot \mathbf{U}_{*\mathbf{R}}^{\mathrm{Roe}} + (1-f) \cdot \mathbf{U}^{\mathrm{HLL}} \tag{56b}$$

where

$$\mathbf{U}_{*\mathbf{L}}^{\mathrm{Roe}} = \mathbf{U}_{\mathbf{L}} + \tilde{\alpha}_1\tilde{\mathbf{K}}^{(1)}, \quad \mathbf{U}_{*\mathbf{R}}^{\mathrm{Roe}} = \mathbf{U}_{\mathbf{R}} - \tilde{\alpha}_4\tilde{\mathbf{K}}^{(4)} \tag{57}$$

4.6. HLLC and Roe schemes with HLLE blending in MUSCL formulation

Using the MUSCL-Hancock scheme, high-order extension is achieved by reconstructed data. Hence, the HLL or HLLE blending technique is applied directly into the HLLC and Roe schemes.

5. HARTEN–HYMAN ENTROPY FIX AUGMENTED BY HLL-TYPE SCHEME

Quirk pointed out that the basic form of the Roe scheme is unable to cope with the test problem of a strong shock diffracting around a corner [3]. As already described in Section 2.3, the entropy

DOI: 10.1002/fld

violating condition is the main drawback of the Roe scheme. The common fix for this problem is to use Harten's classical entropy fix. However, Harten entropy fix is also applied to the contact waves and has a similar effect to our method in Section 4.2. The entropy violating condition of the Roe scheme is associated with the nonlinear fields, since there are no entropy considerations in a linearly degenerate field. The Harten–Hyman entropy fix controls the rarefaction waves only by introducing an intermediate state that has continuous changes. Therefore, we adopted the Haten–Hyman entropy fix.

The proposed blending function surely catches points where the expansion wave is strong, but HLLE blending does not guarantee a stable solution. At these points, especially at corners, the blending function f has a value of about 0.2. Even when f is given a value of 0.0, the Roe scheme fails with Toro's version of the Harten–Hyman entropy fix when the shock turns at the corner. A dissipative scheme blending method controls the magnitude of the flux difference across the middle wave. Thus, it is associated with linear characteristic fields. However, the Harten–Hyman entropy fix modifies the left or right rarefaction wave speeds and is associated with nonlinear fields. Therefore, the blending method does not seem to be suitable in this situation. Therefore, another simple method is suggested when the Harten–Hyman entropy fix of the Roe scheme fails. Quirk employed the HLLE scheme along the sonic lines and strong expansion region [3]; therefore, the HLLE scheme is used across very wide region.

Now we propose a certain criterion as to whether the Harten–Hyman entropy fix fails or not. To use Toro's version of the Harten–Hyman entropy fix, we must obtain star values to estimate the head and tail rarefaction waves (see Figure 2).

The relation of data difference for the left transonic rarefaction case is [1, 13]

$$\mathbf{U}_{*L} - \mathbf{U}_L = \tilde{\alpha}_1 \tilde{\mathbf{K}}^{(1)} \tag{58}$$

The head and tail rarefaction waves are obtained from the particle velocity u_* and sound speed a_{*L}. To estimate the sound speed, pressure or temperature is required.

Internal energy in the star region is obtained as

$$e_{*L} = \frac{1}{\rho_L^*}[\rho_L E_L + \tilde{\alpha}_1(\tilde{H} - \tilde{u}_n \tilde{a})] - \frac{1}{2}(u_{nL}^{*2} + u_{tL}^{*2}) \tag{59}$$

Pressure or temperature in the star region is easily obtained from e_L^*, and the sound speed is calculated using thermodynamic relations. Here, we can set pressure or temperature limits. User-defined limits need not be the actual values. A fairly wide range of limits gives good results. We used temperature limits from 50 to 5000 K. When the resulting temperature deviates from the ranges, we can use full HLLE scheme switching. The HLLC scheme can also be used as a switching scheme to the Roe scheme without sacrificing the exact capturing of contact and shear waves. The HLLC scheme has a shock instability problem, but there is no problem at this strong expansion point. The HLLC and HLLE schemes have the property of preserving positivity. When the HLLC scheme is used as a switching scheme, additional wave speed estimation steps are required. Because the HLLC and Roe schemes are expressed in the same framework using the WAF scheme (Equations (28) and (36)), only $\mathbf{F}_{*\mathbf{L}}$ and $\mathbf{F}_{*\mathbf{R}}$ are changed. Figure 8 shows the detailed procedure of the Haten–Hyman entropy fix augmented by the HLL-type scheme. Figure 9 shows the results of the supersonic corner problem using the first-order accurate Roe scheme with Harten–Hyman entropy fix using HLLE switching. Figure 9(b) shows the points where the entropy fix is required. A parallel line at the corner is the region where the expansion is strong and the

DOI: 10.1002/fld

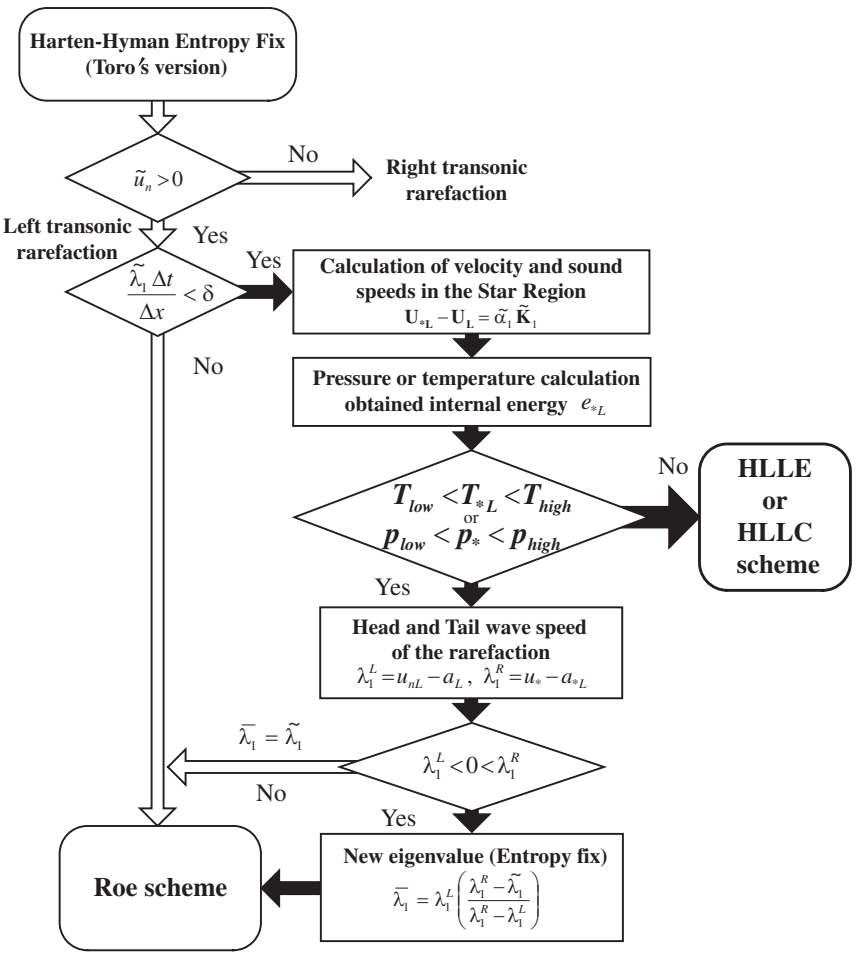

Figure 8. Harten–Hyman entropy fix with HLLC/HLLE switching.

expansion shock can appear. By tracking the HLLE switching points, only one or two points are required at the corner for HLLE switching with the entropy fix.

6. NUMERICAL RESULTS

All the numerical computations are conducted with a CFL number of 0.5. Shock-stable schemes that are blended with dissipative schemes are named as HLLC–HLL and Roe–HLLE. Every result in each test problem is printed at the same time level.

DOI: 10.1002/fld

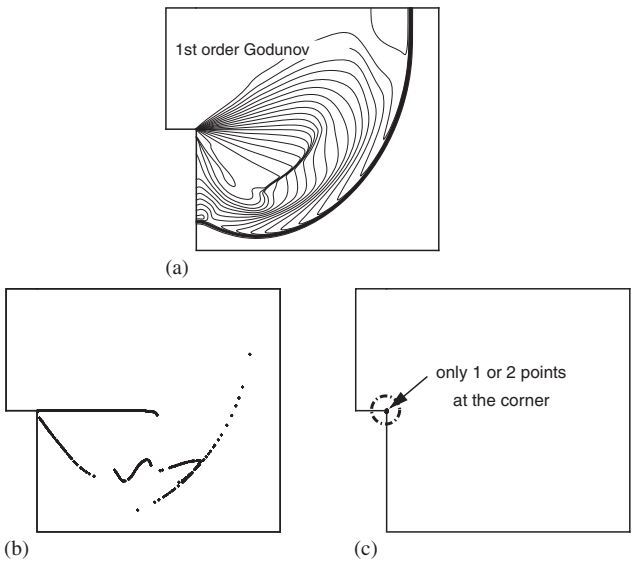

Figure 9. Supersonic corner problem using Harten–Hyman entropy fix with HLLE switching (first-order Godunov): (a) Roe scheme; (b) Harten–Hyman entropy fix; and (c) HLLE switching points.

6.1. Odd–even decoupling

Figure 10 shows Quirk's odd–even decoupling test problem [3]. All the results show the density contour at $X_s \sim 300$. Original schemes that resolve the contacts—HLL and Roe schemes—show the promotion of odd–even decoupling along the shock. However, the HLLE scheme is free from decoupling. Using blending function f, HLLC–HLL and Roe–HLLE show that decoupling is completely eliminated. In these cases, blending function f has a value of about 0.55 along the shock. Figure 11 shows the second-order results of approximate Riemann solvers using WAF schemes with a MINBEE(Minmod) limiter. Figure 12 shows the second-order results of approximate Riemann solvers using MUSCL-Hancock schemes with a MINBEE(Minmod) limiter. When the high-order scheme is used, pressure gradients at cell interfaces have sharper values, and the resulting blending function has a value of about 0.3.

6.2. The carbuncle phenomenon

The carbuncle problem has been observed and discussed for many years. It is considered as a typical example of shock instability. The carbuncle phenomenon was first observed by Peery for blunt body simulations using the Roe scheme [2]. When supersonic or hypersonic blunt body flow is simulated, spurious solutions can appear along the stagnation line. There are nonphysical recirculation regions and a protuberance grows ahead of the bow shock. Some researchers overcome this phenomenon using an entropy fix [2, 6, 7]. However, it is a convenient method to add an artificial dissipation into the scheme [3]. Figures 13–16 show the numerical results of supersonic sphere flows. The freestream Mach number is 5.7, and the grid size is 250×200. In Figure 13, the HLLC scheme shows a sawtooth-like shock front, and a protuberance does not grow. However, nonphysical recirculation is generated at the stagnation point. The Roe scheme shows a typical

DOI: 10.1002/fld

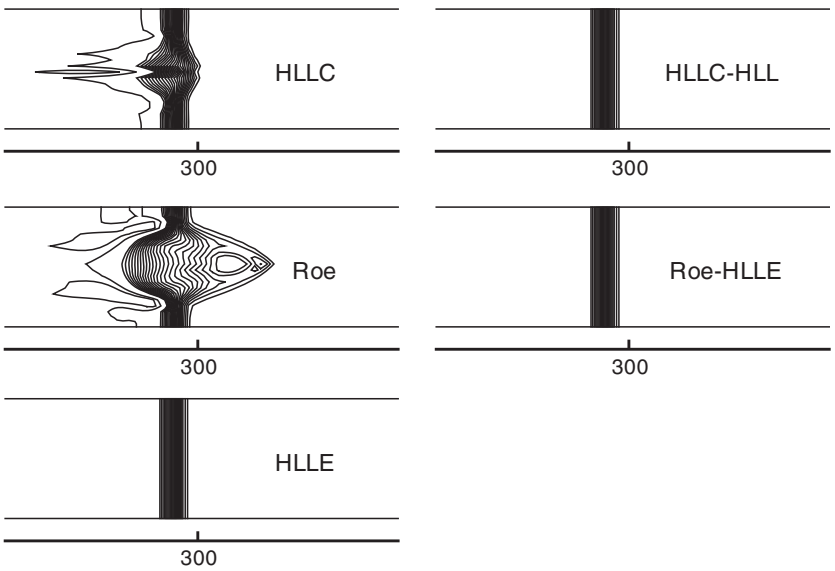

Figure 10. Odd–even grid perturbation problem (first-order Godunov). Left: original schemes, Right: shock stable schemes.

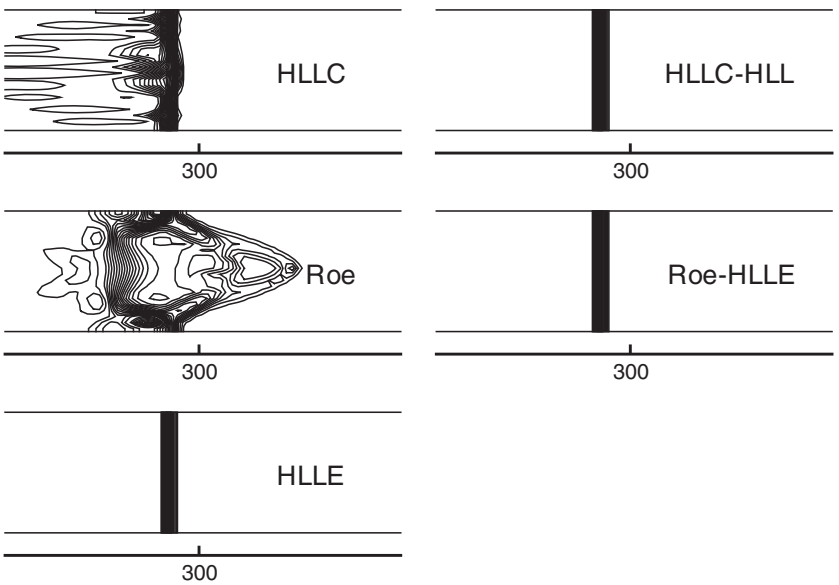

Figure 11. Odd–even grid perturbation problem (second-order WAF with MINBEE (Minmod) limiter).

DOI: 10.1002/fld

Figure 12. Odd–even grid perturbation problem (second-order MUSCL with MINBEE (Minmod) limiter).

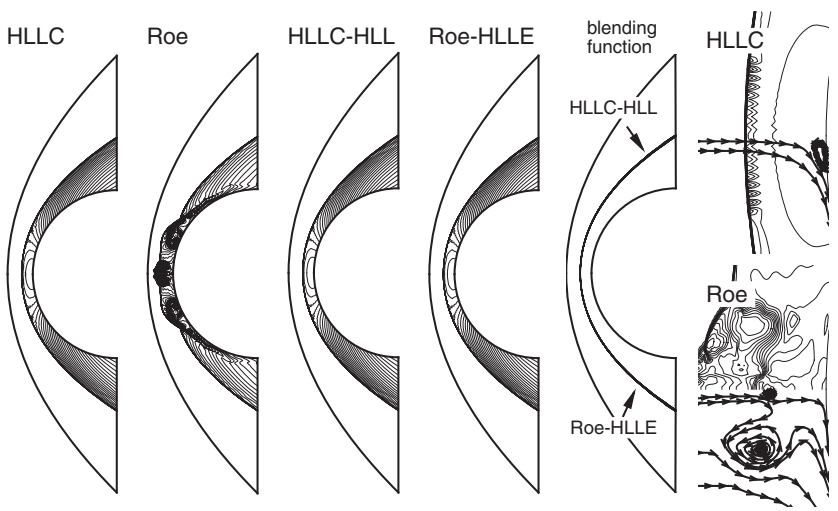

Figure 13. Supersonic sphere flow, density, and blending function distribution (second-order WAF with MINBEE (Minmod) limiter).

carbuncle phenomenon and failed. The carbuncle phenomenon is not shown in HLLC–HLL and Roe–HLLE. Pressure, temperature, and the total enthalpy profile along the stagnation line in Figure 14 show good results. Figures 15 and 16 show numerical results with MUSCL schemes. Results in the stagnation region are somewhat different with WAF schemes, but they show similar results.

The blending function is activated along the shock wave, and is used at only 1% of the total computational domain.

6.3. Kinked Mach stem

When a plane shock is reflected from a ramp, a double-Mach reflection (DMR) is formed if the interaction between the shock wave reflection and the shock-induced flow deflection process is strong. When a DMR is formed, the primary Mach stem is sometimes kinked, similar to the carbuncle phenomenon. Figures 17 and 18 show numerical results of the kinked Mach stem test problem. A planar moving shock has a speed of $M_s = 5.5$ and the ramp angle is 30°. The grid size is 401×401. The original HLLC and Roe schemes in Figures 17 and 18 show the kinked primary Mach stem and it affects the secondary reflected shock from the secondary triple point. Using the

DOI: 10.1002/fld

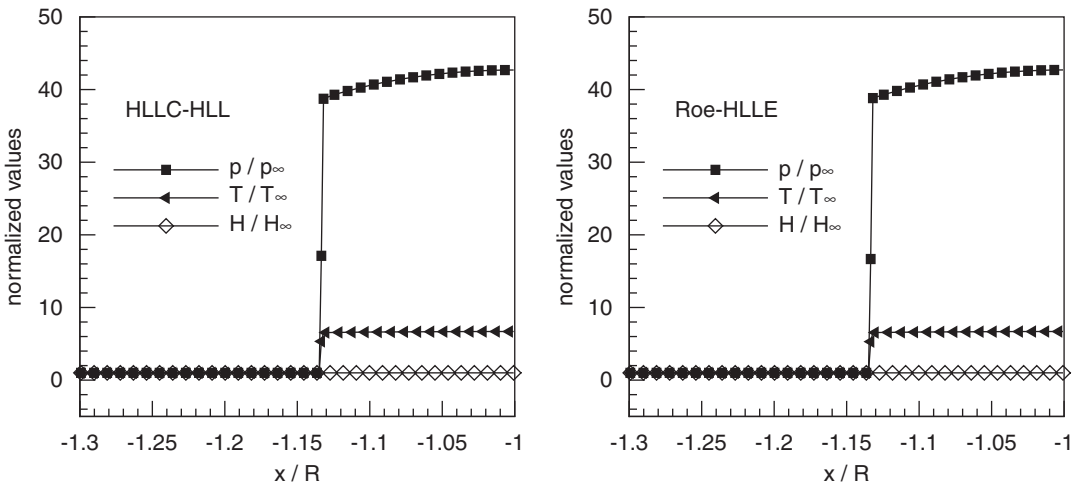

Figure 14. Pressure, temperature, and total enthalpy profile along the stagnation line of supersonic sphere flow (second-order WAF with MINBEE (Minmod) limiter).

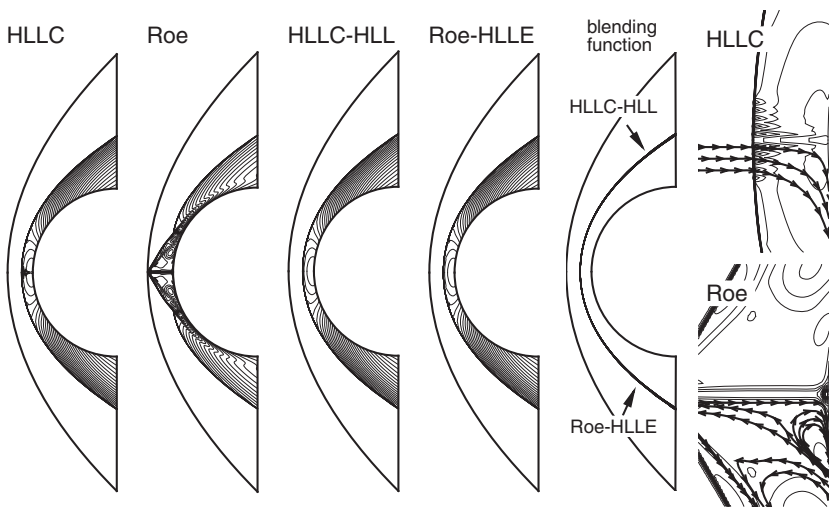

Figure 15. Supersonic sphere flow, density, and blending function distribution (second-order MUSCL with MINBEE (Minmod) limiter).

blending function f, the spurious kinked Mach stem is completely eliminated. Figure 19 shows the blending function distributions, and function f catches only strong shock waves, the moving shock, the primary Mach stem, and the end of the curved part of the reflected shock. There is an incipient odd–even decoupling, where the incident shock crosses the upper boundary for both the HLLC and Roe schemes in Figures 17 and 18. The shock instability is more likely to appear in a high-resolution simulation. Figure 20 shows the higher-resolution results. The grid size is

DOI: 10.1002/fld

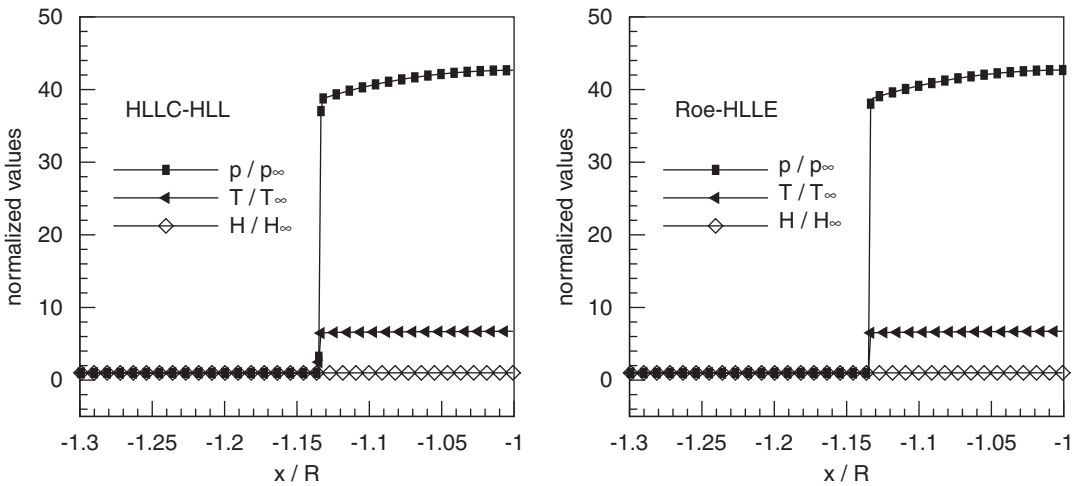

Figure 16. Pressure, temperature, and total enthalpy profile along the stagnation line of supersonic sphere flow (second-order MUSCL with MINBEE (Minmod) limiter).

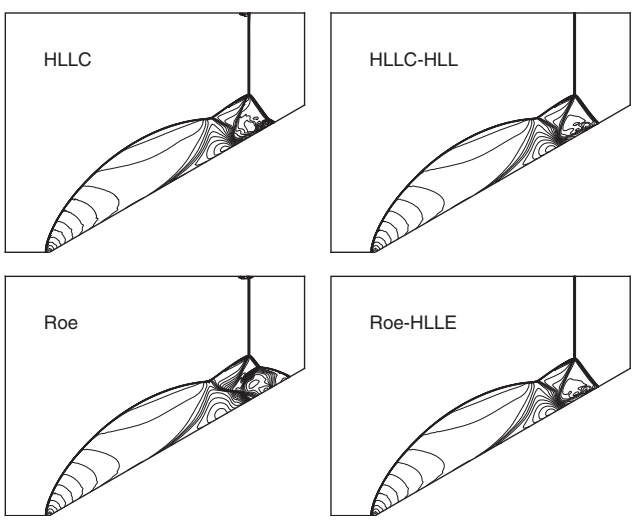

Figure 17. Kinked Mach stem problem, density contour (second-order WAF with MINBEE (Minmod) limiter).

801×801. The spurious primary Mach stem and the incipient odd–even decoupling near the upper wall are more clearly seen.

One may have a suspicion that the additional dissipation of the HLLC–HLL and Roe–HLL can smear intermediate waves such as slip surfaces. The kinked Mach stem problem is a good example to discuss this issue. As shown in Figure 19, additional dissipation is added along the incident shock and the primary Mach stem. The primary slip surface is directly connected to the incident

DOI: 10.1002/fld

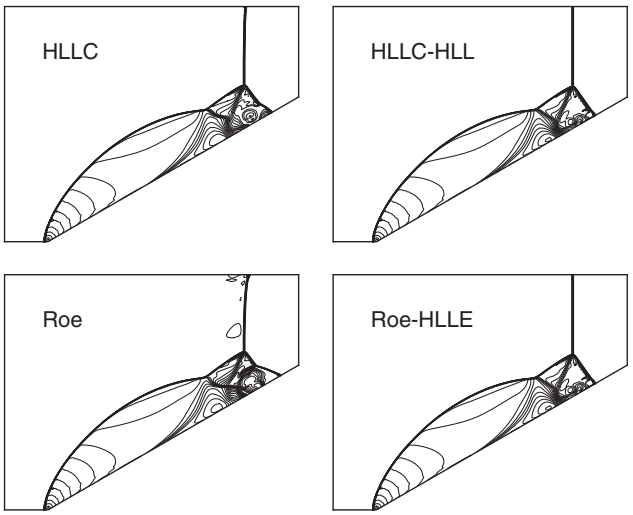

Figure 18. Kinked Mach stem problem, density contour (second-order MUSCL with MINBEE (Minmod) limiter).

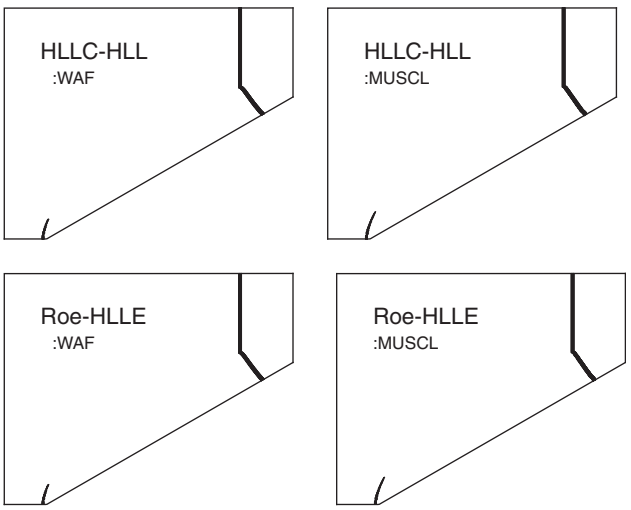

Figure 19. Blending function distribution of the kinked Mach stem problem.

shock and the primary Mach stem. As shown in Figures 17, 18, and 20, the primary slip surface at this triple point shows good resolution. Therefore, local addition of the dissipation has no adverse effect on the resolution of such waves.

DOI: 10.1002/fld

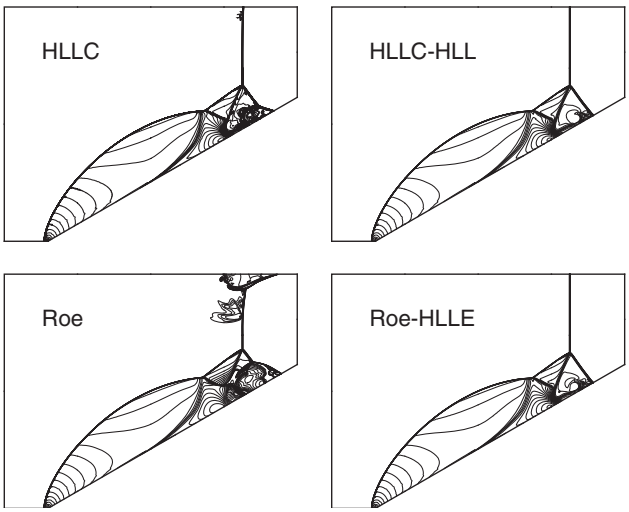

Figure 20. Higher-resolution results of the kinked Mach stem problem, density contour (second-order WAF with MINBEE (Minmod) limiter).

6.4. The supersonic corner flow

Figure 21 shows the results of the supersonic corner problem. A moving shock with $M_s = 5.09$ diffracts around a 90° corner. The grid size is $51 \times 201 + 401 \times 401$. The HLLC scheme has no problem at the corner, but spurious oscillations are observed at the planar moving shock. The Roe scheme still fails near the diffraction shock in high-resolution calculations. Without the use of HLLE blending, the Roe scheme fails in high-order calculation. Roe–HLLE using the Haten–Hyman entropy fix with HLLC/HLLE switching shows stable solutions. Figure 22 shows the distributions of the blending function. HLLC/HLLE blending is activated on the step corner and step wall at the end region of the sonic line where the expansion is strong. The blending function also catches the shock waves.

7. CONCLUSION

Approximate Riemann solvers that resolve contact and shear waves have flaws, so-called shock instabilities, in the vicinity of strong shocks. HLLC and Roe schemes are tested using Quirk's test problems and shock instability appears in both schemes. To avoid this nonphysical result, we propose the control method of flux difference across the contact and shear waves in the star region between the smallest and largest waves. The HLLC and Roe schemes are expressed in a single framework and the proposed method is applied directly. This method is valid for strong shocks, and a function is defined to capture strong shocks.

The odd–even decoupling and the carbuncle phenomenon are successfully controlled with our method. The results of DMR flows show that our method has no adverse effect on the resolution of the intermediate waves such as slip surfaces.

DOI: 10.1002/fld

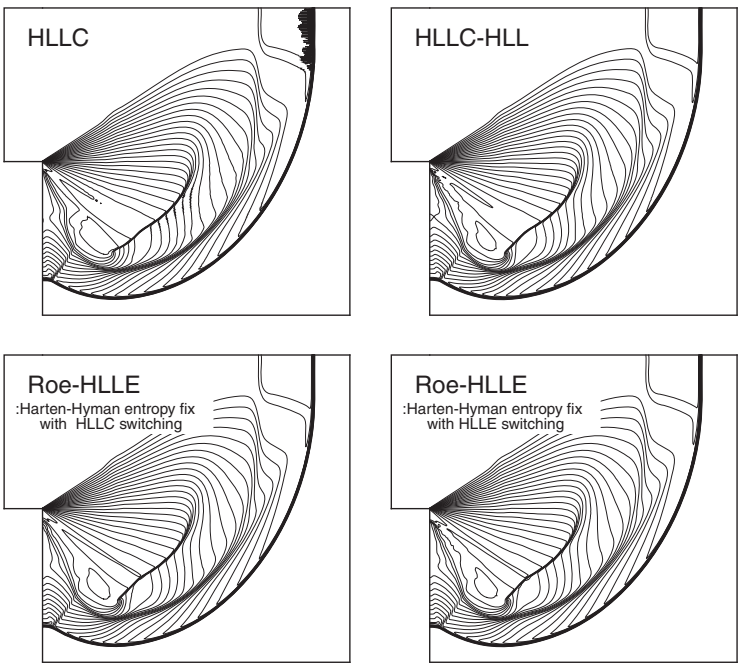

Figure 21. Supersonic corner flow, density distribution (second-order WAF with MINBEE (Minmod) limiter).

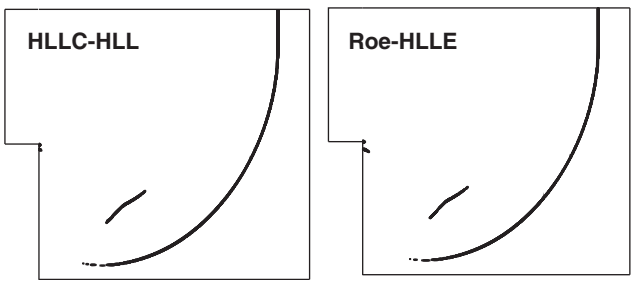

Figure 22. Blending function distribution of supersonic corner flow.

The Roe scheme has another flaw for strong expansion flows. A modified Harten–Hymann entropy fix method is suggested, which uses HLL-type scheme switching. In the supersonic corner flow test, the modified entropy fix worked successfully and spurious oscillations are eliminated at the planar moving shock.

The numerical results with HLLC–HLL and Roe–HLLE show that the shock instability is strongly dependent on the contact resolving properties. Using the control method of flux difference across the contact and shear waves, contact resolving schemes can be free from spurious numerical instabilities.

DOI: 10.1002/fld

ACKNOWLEDGEMENTS

This work was supported by the second stage of the Brain Korea 21 Project in SNU and the Korea Science and Engineering Foundation (KOSEF) grant funded by the Korea government (MEST) (No. R01-2008-000-12362-0).

REFERENCES

1. Toro EF. *Riemann Solvers and Numerical Methods for Fluid Dynamics*. Springer: Berlin, 1999.
2. Peery KM, Imlay ST. Blunt-body flow simulations. *24th SAE ASME and ASEE Joint Propulsion Conference*, *AIAA Paper 88-2904*, Boston, MA, July 1988.
3. Quirk JJ. A contribution to the great Riemann solver debate. *International Journal for Numerical Methods in Fluids* 1994; **18**:555–574.
4. Einfeldt B, Munz CD, Roe PL, Sjogreen B. On Godunov-type methods near low density. *Journal of Computational Physics* 1991; **92**:273–295.
5. Kim SS, Kim C, Rho OH, Hong SK. Cure for the shock instability: development of a shock-stable Roe scheme. *Journal of Computational Physics* 2003; **185**:342–374.
6. Lin HC. Dissipation additions to flux-difference splitting. *10th AIAA Computational Fluid Dynamics Conference*, *AIAA Paper 91-1544*, Honolulu, HI, June 1991.
7. Sanders R, Morano E, Druguet M. Multidimensional dissipation for upwind schemes; stability and applications to gas dynamics. *Journal of Computational Physics* 1998; **145**:511–537.
8. Liou MS. Mass flux schemes and connection to shock instability. *Journal of Computational Physics* 2000; **160**:623–648.
9. Harten A, Lax PD, van Leer B. On upstream difference and Godunov-type schemes for hyperbolic conservation laws. *SIAM Review* 1983; **25**(1):35–61.
10. Toro EF, Spruce M, Speares W. Restoration of the contact surface in the HLL-Riemann solver. *Shock Waves* 1994; **4**:25–34.
11. Batten P, Clarke N, Lambert C, Causon DM. On the choice of wave speeds for the HLLC Riemann solver. *SIAM Journal on Scientific Computing* 1997; **18**(6):1553–1570.
12. Drikakis D, Rider W. *High-resolution Methods for Incompressible and Low-speed Flows*. Springer: Berlin, 2005.
13. Roe PL. Approximate Riemann solvers, parameter vectors, and difference schemes. *Journal of Computational Physics* 1981; **43**:357–372.
14. Roe PL. Characteristic-based schemes for the Euler equations. *Annual Review of Fluid Mechanics* 1986; **18**: 337–365.
15. Quirk JJ. An adaptive grid algorithm for computational shock hydrodynamics. *Ph.D. Thesis*, Cranfield Institute of Technology, 1991.
16. Harten A, Hyman JM. Self adjusting grid methods for one-dimensional hyperbolic conservation laws. *Journal of Computational Physics* 1983; **50**:235–269.
17. Batten P, Leschziner MA, Goldberg UC. Average-state Jacobians and implicit methods for compressible viscous and turbulent flows. *Journal of Computational Physics* 1997; **137**:38–78.
18. Toro EF. A weighted average flux methods for hyperbolic conservation laws. *Proceedings of the Royal Society of London*, *Series A*, *Mathematical and Physical Sciences* 1989; **423**(1865):401–418.
19. Toro EF. The weighted average flux method applied to the Euler equations. *Philosophical Transactions*: *Physical Sciences and Engineering* 1992; **341**(1662):499–530.
20. Billett SJ, Toro EF. On WAF-type schemes for multidimensional hyperbolic conservation laws. *Journal of Computational Physics* 1997; **130**:1–24.
21. Billett SJ, Toro EF. Unsplit WAF-type schemes for three dimensional hyperbolic conservation laws. *Numerical Methods for Wave Propagation*. Kluwer Academic Publishers: Dordrecht, 1998; 75–124.
22. Pandolfi M, D'Ambrosio D. Numerical instabilities in upwind methods: analysis and cures for the 'Carbuncle' phenomenon. *Journal of Computational Physics* 2001; **166**:271–301.

DOI: 10.1002/fld